Direct multi-elemental imaging of freshly impregnated catalyst by Laser-Induced Breakdown Spectroscopy

Lina Jolivet, Leonor Catita, Olivier Delpoux, Charles-Philippe Lienemann, Loïc Sorbier, Vincent Motto-Ros

Direct multi-elemental imaging of freshly impregnated catalyst by Laser-Induced Breakdown Spectroscopy

Lina Jolivet,[#§] Leonor Catita,[#] Olivier Delpoux, [#] Charles-Philippe Lienemann,[#] Loïc Sorbier,[#] Vincent Motto-Ros[§]

[#]IFP Energies nouvelles, Rond-Point de l'échangeur de Solaize, BP 3, 69360 Solaize, France

[§]Institut Lumière Matière UMR 5306, Université Lyon 1 - CNRS, Université de Lyon 69622 Villeurbanne, France

KEYWORDS LIBS imaging, Alumina, catalyst, impregnation, additive

ABSTRACT

The preparation step of a catalyst is of primary importance as it may govern its performance. We report here the first direct multi-elemental imaging of an alumina-supported catalyst during the maturation process. Alumina extrudate support was impregnated with a nickel nitrate solution in the presence of citric acid as an organic additive. Wet extrudates were sampled, cut in half and imaged by Laser-Induced Breakdown Spectroscopy (LIBS) for varying maturation times. Results were validated by comparison with more conventional techniques such as Raman and Magnetic Resonance Imaging. This communication demonstrates the speed of acquisition, low detection limits and multi-elemental capabilities of LIBS to provide valuable information to understand the phenomena occurring during catalyst impregnation. The

proposed approach allows one to shorten drastically the analysis time (by a factor of 30) and emphasizes LIBS imaging potential as a unique characterization technique able to simultaneously monitor the distribution of the metallic precursor, organic additive and support impurities.

INTRODUCTION

The preparation step of a heterogeneous catalyst is of paramount importance to control how the active phase is dispersed on the support surface and distributed within the support [1]. These latter properties may directly influence the catalyst performance and thus catalytic processes efficiency. Most of the industrial catalysts are prepared through incipient wetness impregnation. Active phase precursors are dissolved in a solution, sometimes with an additive. Dry support is then put in contact with a volume of this solution equal to the support porous volume. After impregnation, the catalyst is left to mature for a sufficient-time to allow the precursors to diffuse into the core. Matured catalyst is then dried, sometimes calcined, and activated before use. Studying the maturation step of the catalyst is of utmost importance for two reasons. First, in order to understand and rationalize the phenomena arising at this step, to adjust solution and support characteristics (kind of precursor and solvent, concentration of precursors, presence of additives, specific surface area and porous volume of the support, etc.) to finally obtain the desired dispersion and distribution of the active phase. Second, the maturation step governs the efficiency of the industrial catalyst production line. On that purpose, several characterization techniques have been employed such as Raman imaging [2,3], Magnetic Resonance Imaging (MRI) [3–10] or UV-visible spectroscopy [2,3,11]. All these techniques have shown serious limitations when applied to maturation process investigation. MRI is an indirect method, with difficulties of image interpretation for multi-elemental impregnation solutions. Besides, MRI and Raman require quite long acquisition times, which makes

these techniques not suitable for the study of fast kinetics phenomena, for example the redistribution of species within the support. Other methods such as selective scratching of the catalyst beads [12], optical microscopy [13–15] or X-ray energy dispersive spectrometry [16] require sample drying or calcination before measuring elemental distribution, which may induce several transformations, such as decomposition of the active precursors, formation of new surface species and redistribution effects. Different models for dry or wet impregnation of catalysts have been proposed [10,12–18] in order to simulate the final active phase distribution. Some of them take into account competitive impregnation [15,17]. The availability of direct, fast, and multi-elemental spatially resolved characterization techniques is of primary importance for validation and improvement of such models.

Recently, laser-induced breakdown spectroscopy (LIBS) has emerged as a promising characterization technique providing fast and multi-elemental imaging with high sensitivity and relevant spatial resolution to characterize the precursors and additive distribution at the catalyst's bead scale [19,20]. Besides, this technique offers the possibility to operate under ambient conditions. LIBS imaging has been already successfully applied to characterize elemental distribution on calcined [21] or dried [22] catalyst surface. This communication reports the very first application of LIBS imaging on a maturating supported catalyst. A nickel based catalyst supported on γ-alumina in the presence of an organic additive (here citric acid) was chosen as a model system to exemplify this methodology. LIBS images were validated by comparison with MRI and Raman imaging. This work aims to emphasize LIBS potential as a unique characterization technique to simultaneously monitor the transport of the metallic precursor and organic additive at the very initial times of the maturation stage, which can give new insights to optimize the preparation step of heterogeneous catalysts.

MATERIALS AND METHODS

Impregnation solution and support

A solution of nickel nitrate $Ni(NO_3)_2.6H_2O$ (Sigma-Aldrich, 98.5% purity) in deionized water was prepared to obtain a concentration of [Ni]=0.05 mol/L for nickel. Citric acid (CA) (Sigma-Aldrich, 99.5% purity) was added to this solution to obtain two impregnation solutions of [CA]=0.06 mol/L and [CA]=0.2 mol/L for citric acid. A single mesoporous γ-Al_2O_3 trilobed extrudate of 1.2−1.3 mm diameter and 6 mm length, 0.6 cm^3/g porous volume and 250 m^2/g specific surface area was immerged during 30 s in 20 ml of the impregnation solution. The extrudate was removed from the solution, wiped with absorbent paper, and left to mature for a given maturation time T_M. The extrudate was cut in half, perpendicularly to the direction of extrusion with a scalpel, and one of the half-extrudate was set aside to be imaged by LIBS. The procedure was repeated for different extrudates, different maturation times ranging from 30 s to 23 h and for both impregnation solutions. Such procedure mimics the incipient wetness impregnation procedure while being easier to perform and more reproducible for single extrudates preparation.

LIBS imaging

The half extrudate was positioned on the LIBS sample holder with modeling paste so that the fresh cut surface was horizontal and upwards. The LIBS instrument used in this study has already been described in detail in a previous article [23]. A nanosecond Nd:YAG laser source was employed, operating at a 100 Hz repetition rate and emitting in the fundamental wavelength (1064 nm). The laser beam was focused vertically into the sample surface by a 15× magnification objective. The laser energy was set at 1.5 mJ leading to a typical crater size of less than 15 µm. Extrudates were scanned with the help of a motorized xyz stage. A 15 µm step size was used by adjusting the motor speed according to the fixed laser repetition rate. Images of a single extrudate were 142×120 pixels wide and were acquired in 170 s. Homemade software developed in the LabVIEW environment controlled the whole system and allowed automated

sequences in order to scan the region of interest. The plasma radiation was collected by two lens-fiber systems, positioned with an angle of 35° relative to the sample surface. The outputs of the fibers were connected to two independent Czerny-Turner spectrometers, a Shamrock 500 (Andor Technology) and a Shamrock 303 (Andor Technology). Each of these spectrometers was equipped with an intensified CCD camera (iStar, ICCD, Andor Technology). The spectral acquisition was performed by the synchronization between the Q-switch of laser and the ICCD cameras. All experiments were carried out in ambient atmosphere with an argon gas flowing the plasma region (1.6 L/min) to both improve the signal to noise ratio and prevent any surface contamination by ablated material deposition from previous laser shots. Selected emission lines of each element of interest are summarized in supplementary Table 1. On each pixel of an extrudate image, the net intensity of a given emission line was obtained by subtracting the emission background on a spectral window, far from any emission line, from the intensity on a spectral window centered around this emission line.

MRI

A wiped extrudate was placed vertically in a 1.7 mm diameter capillary tube further inserted in a 5 mm NMR tube. MRI experiments were performed in a Bruker Avance 400 MHz (^{1}H) spectrometer equipped with a 5 mm imaging probe (Micro5) and xyz gradient amplifiers (300 × 300 × 300 G/cm) at 60 A current, which allowed selecting the voxels of interest. Experiments were carried out at a temperature of 17 °C. Axial-oriented images were obtained using a spin-echo sequence, which consists of a π/2 pulse of 22.5 µs length followed by a π pulse. A field of view of 2.5 × 2.5 × 8 mm and 64 × 64 × 8 acquisition points was chosen, resulting in a voxel size of 39 µm × 39 µm × 1000 µm. A slice thickness of 1 mm was defined. For each MRI experiment, 8 images were obtained, each one corresponding to a certain position along the z axis of the pellet. Only the images corresponding to the central z axis slice will be shown. The transport of nickel and citrate ions was monitored simultaneously using the ^{1}H MRI method reported earlier [3,4].

As a result of the repetition time (T_R) and echo time (T_E) chosen (500 ms and 2.5 ms, respectively), protons near nickel ions are observed thanks to a T_2 contrast (long T_E comparing to the T_2 of protons close to Ni), while protons near citric acid were observed thanks to a T_1 contrast (small T_R comparing to T_1 of protons close to the organic additive). Using such parameters, low or even null pixel intensity corresponds to high Ni local concentration, whereas high pixel intensities are attributed to a higher citric acid local concentration in respect to Ni local concentration. The shorter image acquisition time for all volumes was 17 min. Relaxation times were measured using Rapid Acquisition with Relaxation Enhancement with variable repetition time T_R sequence (RARE) [24]. Proton T_1 and T_2 of pure water inside γ-Al_2O_3 support was 370 ms and 4 ms, respectively. In the presence of nickel ions, these values were decreased to approximately 15 ms and 2 ms, respectively, at the lowest Ni concentration used. On the contrary, T_1 value is increased to 470 ms in the presence of citric acid at the lowest CA concentration used, while the T_2 value remained almost the same (4 ms). Paravision 5.1 software was used for ^{1}H MRI images acquisition.

Raman

A half wiped extrudate was positioned with the fresh cut surface upwards in a Renishaw inVia Reflex Raman microscope. Excitation line of 532 nm wavelength and 3.5 mW power was provided by a Nd:YAG laser fitted with EasyConfocal Renishaw device. The scattered light was dispersed with a 2400 lines/mm grating leading to a spectral resolution around 0.9 cm^{-1}. Raman images were acquired in the Streamline mode [25] with 60 s exposure and 16.2 µm × 16.2 µm pixel size. The shorter acquisition time of a spectral image lasted 9 h. The band at 1417 cm^{-1}, ascribed to the stretching vibrations of carboxylate group (COO^-) [26], allowed citrate distribution imaging from the intensity at 1417 cm^{-1}.

RESULTS

Nickel and carbon imaging

LIBS intensities images for nickel (Ni) and carbon (C) together with ^{1}H MRI images and citrate Raman images are reported in Figure 1. Similar behaviour is observed for both impregnation solutions. Carbon is distributed in a corona around the extrudate surface whatever the maturation times, whereas nickel distribution is evolving over maturation time. One can clearly notice the thicker C corona for the more CA concentrated solution. LIBS C elemental distribution is coherent with Raman imaging of citrate and LIBS Ni distribution is in accordance with MRI. During transient regime, one can clearly notice an over-concentration of Ni, just in the internal face of the C layer, and a significant concentration of Ni, overlapping the C layer. Such information could not be extracted from Raman and MRI images. As LIBS mapping is fast (measurement in less than 3 minutes), shorter maturation times were also accessible. In addition, since LIBS measures only the first microns thick upper the sample surface, it is reasonable to assume that the samples are (at least partially) dried at the time the extrudate is cut, before analysis. The observed C and Ni distributions indicate a competitive adsorption mechanism between the active phase precursor and the additive, resulting in a preferential adsorption of citrate ions on the γ-alumina surface in relation to Ni ions. Consequently, egg-shell profiles of C are obtained, while almost uniform Ni profiles are found at long maturation times.

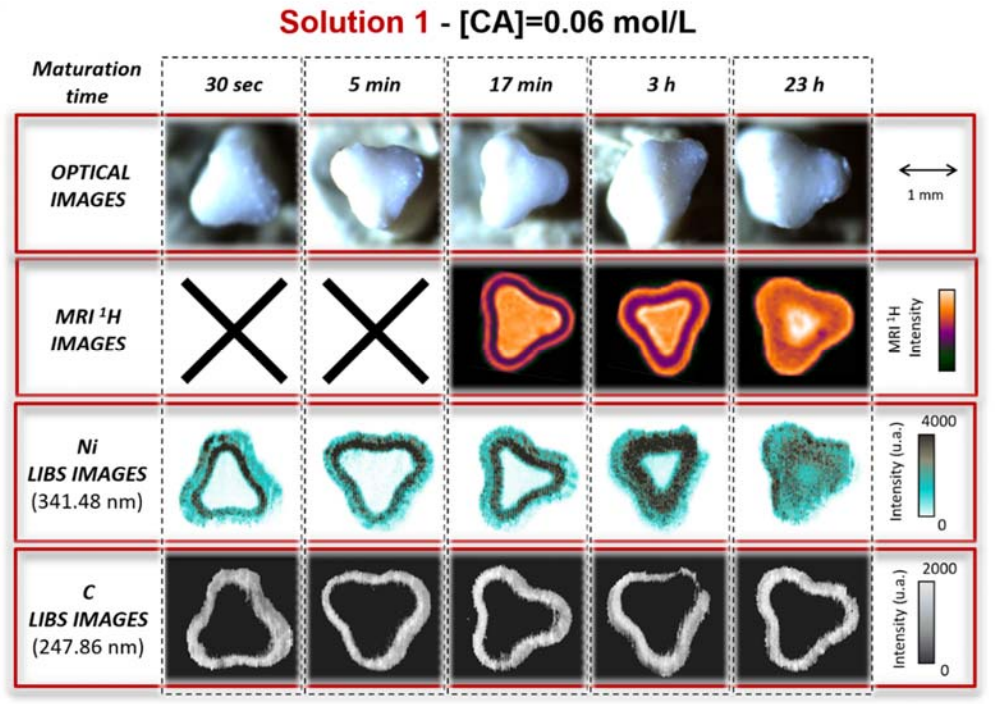
Solution 1 - [CA]=0.06 mol/L
Maturation time
30 sec
5 min
17 min
3 h
23 h
OPTICAL IMAGES
1 mm
MRI ¹H IMAGES
MRI ¹H Intensity
Ni LIBS IMAGES (341.48 nm)
Intensity (u.a.)
4000
0
C LIBS IMAGES (247.86 nm)
Intensity (u.a.)
2000
0

150

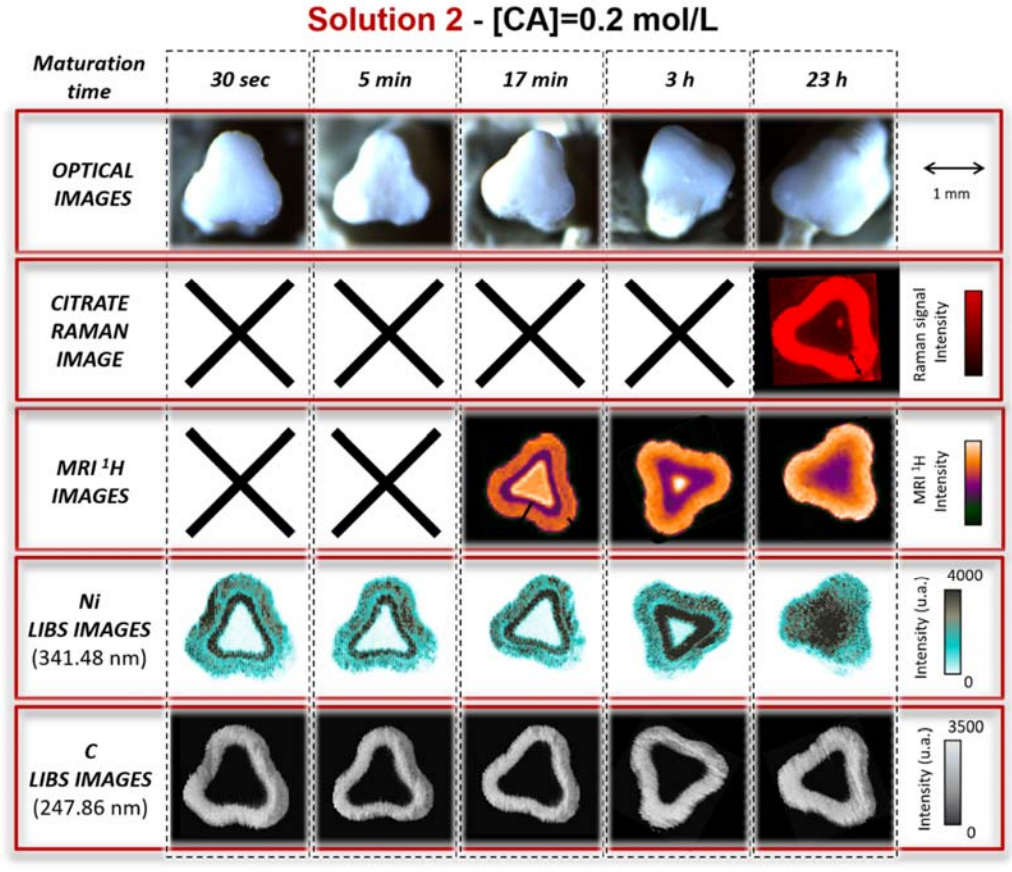
Solution 2 - [CA]=0.2 mol/L
Maturation time
30 sec
5 min
17 min
3 h
23 h
OPTICAL IMAGES
1 mm
CITRATE RAMAN IMAGE
Raman signal Intensity
MRI ¹H IMAGES
MRI ¹H Intensity
Ni LIBS IMAGES (341.48 nm)
Intensity (u.a.)
4000
0
C LIBS IMAGES (247.86 nm)
Intensity (u.a.)
3500
0

151

Figure 1. Ni and C LIBS intensities images, ^{1}H MRI and Raman citrate images for varying maturation times T_M and impregnation solutions.

Support impurities imaging

Figure 2 shows LIBS imaging of support impurities that are displaced during the catalyst maturation. We show for the very first time Mg, Ca and Na distribution evolving during the maturation process. These elements are present in the alumina support and each one has a specific behavior during the impregnation process. As Na seems to remain well distributed regardless the maturation time, Mg and Ca appear to be pushed in the front of the Ni layer. This observation suggests a different strength of interaction with alumina surface (Ca and Mg are less tightly bound to alumina surface than Na) or a different nature (Mg and Ca are on hydroxydes forms which are dissolved by the acid solution whereas Na is not).

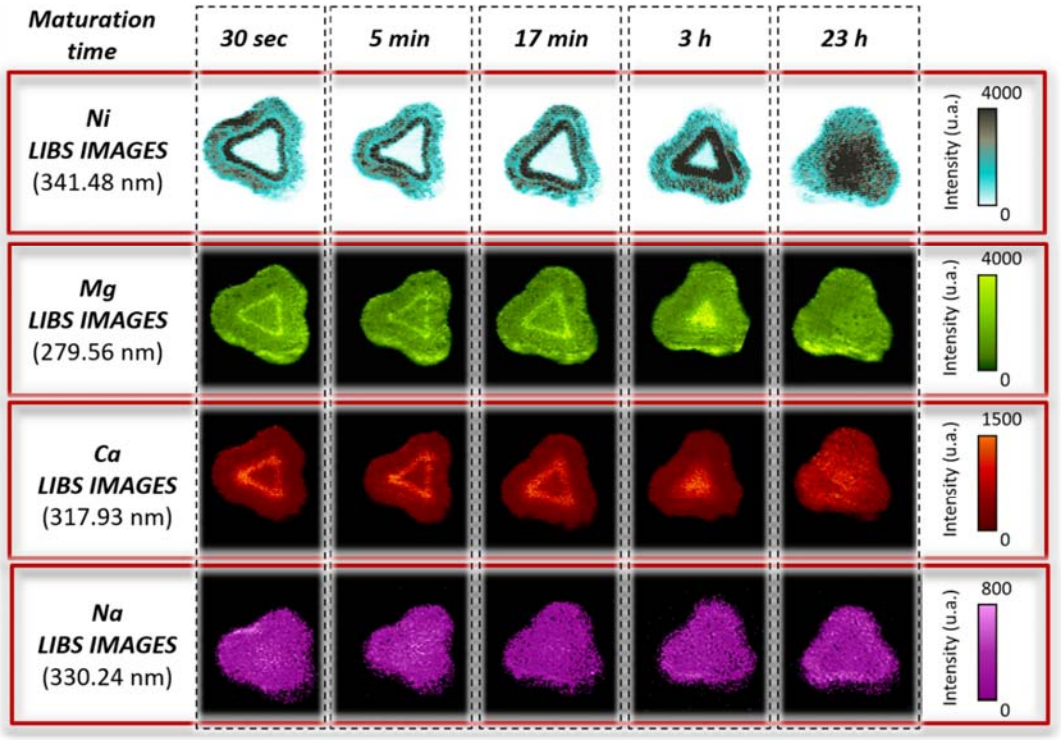

Figure 2. Ni, Mg, Ca, and Na LIBS intensities images for varying maturation times T_M for [CA]=0.2 mol/L.

DISCUSSION

These results show that LIBS imaging technique is particularly suitable to characterize the maturation step of catalysts. LIBS elemental mapping provides a fast and direct analysis of the distribution of the active phase and additive along alumina surface. It is important to notice than both active phase precursor and additive are detected simultaneously with LIBS, allowing a unique and direct characterization of the transport of the metallic precursor and organic additive. Short acquisition times provided by LIBS technique allow the characterization of extrudates in the earliest times of the maturation process (30 s). Until now, such acquisition times were not accessible as the first map could not be obtained before 17 minutes with MRI technique and several hours of acquisition are required to obtain Raman mappings in streamline mode. At the longest maturation times, LIBS imaging is entirely in accordance with MRI and Raman analysis, while revealing relevant new information with regards to the less concentrated species. The multi-elemental capabilities of LIBS combined with its high sensitivity allows one to image the trace impurities that are displaced during the catalyst maturation, involving very low concentrations down to the ppm scale.

CONCLUSION

This work shows the high potential of LIBS imaging technique to image catalysts at different times of the maturation step. Performed at ambient conditions, LIBS enables imaging wet samples without operating issues. Its multi-elemental capabilities allowed us to monitor simultaneously the active phase precursor (Ni) and the organic additive (C) that in the past required the use of different analytical approaches. Its sensitivity revealed the displacement (Mg and Ca) or the strong anchoring (Na) of the support impurities during maturation. Its speed of acquisition (image of an extrudate in less than 3 minutes) enabled studying the early times of the maturation process never accessible until now with conventional

techniques. Such capabilities are expected to be of primary importance for the understanding of phenomena during catalyst preparation and the development of quantitative impregnation models.

ASSOCIATED CONTENT

LIBS optical emission lines used in this study are available as supporting information.

AUTHOR INFORMATION

Corresponding Author

loic.sorbier@ifpen.fr

Author Contributions

L.J.: Investigation, Formal analysis, Validation, Visualization, Writing - Review & Editing

L.C.: Methodology, Investigation, Writing - Review & Editing

O.D.: Methodology, Writing - Review & Editing

C.-P.L.: Conceptualization, Writing - Review & Editing, Supervision

L.S.: Conceptualization, Writing - Original Draft

V.M.-R.: Conceptualization, Methodology, Writing - Review & Editing

ABBREVIATIONS

CA, citric acid, LIBS, laser-induced breakdown spectroscopy, MRI, nuclear magnetic resonance imaging, NMR, nuclear magnetic resonance.

REFERENCES

[1] A.V. Neimark, L.I. Kheifets, V.B. Fenelonov, Theory of preparation of supported catalysts, Ind. Eng. Chem. Prod. Res. Dev. 20 (1981) 439–450. https://doi.org/10.1021/i300003a006.

[2] J.A. Bergwerff, L.G.A. van de Water, T. Visser, P. de Peinder, B.R.G. Leliveld, K.P. de Jong, B.M. Weckhuysen, Spatially resolved Raman and UV-visible-NIR spectroscopy on the preparation of supported catalyst bodies: controlling the formation of H2PMo11CoO40 5- inside Al2O3 pellets during impregnation, Chemistry (Weinheim an der Bergstrasse, Germany) 11 (2005) 4591–4601. https://doi.org/10.1002/chem.200500116.

[3] L. Catita, A.-A. Quoineaud, M. Moreaud, D. Espinat, C. Pichon, O. Delpoux, Impact of Citric Acid on the Impregnation of CoMoP/γ-Al2O3 Catalysts: Time and Spatially Resolved MRI and Raman Imaging Study, Top Catal 61 (2018) 1474–1484. https://doi.org/10.1007/s11244-018-1038-7.

[4] L. Catita, A.-A. Quoineaud, D. Espinat, C. Pichon, O. Delpoux, Application of Magnetic Resonance Imaging and Raman Imaging to study the impact of phosphorus in impregnation of hydrotreatment catalysts, Applied Catalysis A: General 547 (2017) 164–175. https://doi.org/10.1016/j.apcata.2017.08.039.

[5] A. Nowacka, J. Moughames, Z. Adem, A.-A. Quoineaud, M. Rolland, F. Guenneau, A. Gédéon, In situ magnetic resonance imaging study of the impregnation of γ-alumina pellets, Applied Catalysis A: General 503 (2015) 111–116. https://doi.org/10.1016/j.apcata.2015.07.014.

[6] A.A. Lysova, J.A. Bergwerff, L. Espinosa-Alonso, B.M. Weckhuysen, I.V. Koptyug, Magnetic resonance imaging as an emerging tool for studying the preparation of supported catalysts, Applied Catalysis A: General 374 (2010) 126–136. https://doi.org/10.1016/j.apcata.2009.11.038.

[7] L. Espinosa-Alonso, A.A. Lysova, P. de Peinder, K.P. de Jong, I.V. Koptyug, B.M. Weckhuysen, Magnetic resonance imaging studies on catalyst impregnation processes: discriminating metal ion complexes within millimeter-sized gamma-Al2O3 catalyst bodies, Journal of the American Chemical Society 131 (2009) 6525–6534. https://doi.org/10.1021/ja900346k.

[8] J.A. Bergwerff, A.A. Lysova, L. Espinosa Alonso, I.V. Koptyug, B.M. Weckhuysen, Probing the transport of paramagnetic complexes inside catalyst bodies in a quantitative manner by magnetic resonance imaging, Angewandte Chemie (International ed. in English) 46 (2007) 7224–7227. https://doi.org/10.1002/anie.200701399.

[9] A.A. Lysova, I.V. Koptyug, R.Z. Sagdeev, V.N. Parmon, J.A. Bergwerff, B.M. Weckhuysen, Non-invasive in situ visualization of supported catalyst preparations using multinuclear magnetic resonance imaging, Journal of the American Chemical Society 127 (2005) 11916–11917. https://doi.org/10.1021/ja053456v.

[10] L. Catita, E. Jolimaitre, A.-A. Quoineaud, O. Delpoux, C. Pichon, J.-M. Schweitzer, Mathematical modeling and Magnetic Resonance Imaging experimental study of the impregnation step: A new tool to optimize the preparation of heterogeneous catalysts, Microporous and Mesoporous Materials 312 (2021) 110756. https://doi.org/10.1016/j.micromeso.2020.110756.

[11] L.G.A. van de Water, J.A. Bergwerff, T.A. Nijhuis, K.P. de Jong, B.M. Weckhuysen, UV-Vis microspectroscopy: probing the initial stages of supported metal oxide catalyst preparation, Journal of the American Chemical Society 127 (2005) 5024–5025. https://doi.org/10.1021/ja044460u.

[12] O.A. Scelza, A.A. Castro, D.R. Ardiles, J.M. Parera, Modeling of the impregnation step to prepare supported platinum/alumina catalysts, Ind. Eng. Chem. Fund. 25 (1986) 84–88. https://doi.org/10.1021/i100021a012.

[13] R.C. Vincent, R.P. Merrill, Concentration profiles in impregnation of porous catalysts, Journal of Catalysis 35 (1974) 206–217. https://doi.org/10.1016/0021-9517(74)90199-7.

[14] M. Komiyama, R. Merrill, H.F. Harnsberger, Concentration profiles in impregnation of porous catalysts: Nickel on alumina, Journal of Catalysis 63 (1980) 35–52. https://doi.org/10.1016/0021-9517(80)90058-5.

252 [15] P. Papageorgiou, D.M. Price, A. Gavriilidis, A. Varma, Preparation of Pt/γ-Al2O3Pellets with In-
253 ternal Step-Distribution of Catalyst: Experiments and Theory, Journal of Catalysis 158 (1996)
254 439–451. https://doi.org/10.1006/jcat.1996.0045.
255 [16] E. Assaf, L. Jesus, J. Assaf, The active phase distribution in Ni/Al2O3 catalysts and mathematical
256 modeling of the impregnation process, Chemical Engineering Journal 94 (2003) 93–98.
257 https://doi.org/10.1016/S1385-8947(03)00006-8.
258 [17] S.S. Kulkarni, G.R. Mauze, J.A. Schwarz, Concentration profiles and the design of metal-sup-
259 ported catalysts, Journal of Catalysis 69 (1981) 445–453. https://doi.org/10.1016/0021-
260 9517(81)90180-9.
261 [18] X. Liu, J.G. Khinast, B.J. Glasser, A parametric investigation of impregnation and drying of sup-
262 ported catalysts, Chemical Engineering Science 63 (2008) 4517–4530.
263 https://doi.org/10.1016/j.ces.2008.06.013.
264 [19] L. Jolivet, M. Leprince, S. Moncayo, L. Sorbier, C.-P. Lienemann, V. Motto-Ros, Review of the
265 recent advances and applications of LIBS-based imaging, Spectrochimica Acta Part B: Atomic
266 Spectroscopy 151 (2019) 41–53. https://doi.org/10.1016/j.sab.2018.11.008.
267 [20] A. Limbeck, L. Brunnbauer, H. Lohninger, P. Pořízka, P. Modlitbová, J. Kaiser, P. Janovszky, A.
268 Kéri, G. Galbács, Methodology and applications of elemental mapping by laser induced break-
269 down spectroscopy, Analytica chimica acta 1147 (2021) 72–98.
270 https://doi.org/10.1016/j.aca.2020.12.054.
271 [21] F. Trichard, L. Sorbier, S. Moncayo, Y. Blouët, C.-P. Lienemann, V. Motto-Ros, Quantitative ele-
272 mental imaging of heterogeneous catalysts using laser-induced breakdown spectroscopy, Spectro-
273 chimica Acta Part B: Atomic Spectroscopy 133 (2017) 45–51.
274 https://doi.org/10.1016/j.sab.2017.04.008.

[22] F. Trichard, F. Gaulier, J. Barbier, D. Espinat, B. Guichard, C.-P. Lienemann, L. Sorbier, P. Levitz, V. Motto-Ros, Imaging of alumina supports by laser-induced breakdown spectroscopy: A new tool to understand the diffusion of trace metal impurities, Journal of Catalysis 363 (2018) 183–190. https://doi.org/10.1016/j.jcat.2018.04.013.

[23] V. Motto-Ros, E. Negre, F. Pelascini, G. Panczer, J. Yu, Precise alignment of the collection fiber assisted by real-time plasma imaging in laser-induced breakdown spectroscopy, Spectrochimica Acta Part B: Atomic Spectroscopy 92 (2014) 60–69. https://doi.org/10.1016/j.sab.2013.12.008.

[24] J. Hennig, A. Nauerth, H. Friedburg, RARE imaging: a fast imaging method for clinical MR, Magnetic resonance in medicine 3 (1986) 823–833. https://doi.org/10.1002/mrm.1910030602.

[25] R. Bennett, I.P. Hayward, J.E. Smith, Spectroscopic apparatus with dispersive device for collecting sample data in synchronism with relative movement of a focus, US8179526B2 (2012).

[26] R.I. Bickley, H. Edwards, R. Gustar, S.J. Rose, A vibrational spectroscopic study of nickel(II) citrate Ni3(C6H5O7)2 and its aqueous solutions, Journal of Molecular Structure 246 (1991) 217–228. https://doi.org/10.1016/0022-2860(91)80128-Q.

291

292 Supplementary Table 1

Element of interest	Selected emission line (nm)
Ni	341.48
C	247.86
Mg	279.56
Ca	317.93
Na	330.24

293